

Theory of a magnetic microscope with nanometer resolution

Peter Johansson*

*Division of Solid State Theory, Department of Physics, University of Lund, Sölvegatan 14 A, S-223 62 Lund, Sweden
and Department of Natural Sciences, University of Örebro, S-701 82 Örebro, Sweden*

S. Peter Apell†

*Department of Applied Physics, Chalmers University of Technology and Göteborg University, S-41296 Göteborg, Sweden
and Donostia International Physics Center, San Sebastian, Spain*

D. R. Penn‡

*Electron Physics Group, National Institute of Standards and Technology, Gaithersburg, MD 20899, USA
(October 31, 2018)*

We propose a theory for a type of apertureless scanning near field microscopy that is intended to allow the measurement of magnetism on a nanometer length scale. A scanning probe, for example a scanning tunneling microscope (STM) tip, is used to scan a magnetic substrate while a laser is focused on it. The electric field between the tip and substrate is enhanced in such a way that the circular polarization due to the Kerr effect, which is normally of order 0.1% is increased by up to two orders of magnitude for the case of a Ag or W tip and an Fe sample. Apart from this there is a large background of circular polarization which is non-magnetic in origin. This circular polarization is produced by light scattered from the STM tip and substrate. A detailed retarded calculation for this light-in-light-out experiment is presented.

61.16.Ch, 78.20.Ls

I. BACKGROUND

A microscope that can measure magnetic structure with high resolution would be very desirable for practical reasons such as investigating read heads and media for magnetic recording and because magnetic nanostructures are currently of great interest. We propose a scanning magnetic microscope with a resolution of approximately 1 nm to 10 nm¹ depending on the tip shape. This device is a form of apertureless near-field scanning magneto-optical microscope in which light from a laser is focused at the tip of a scanning tunneling microscope (STM) or atomic force microscope (AFM) or at an isolated sphere on the sample surface and the circular polarization of the light scattered from the tip and sample is measured. This is analogous to attempts to use the circular polarization of the light emitted by a scanning tunneling microscope to construct a magnetic microscope.²⁻⁵ It was found that the light-emission scheme is not suitable for use as a magnetic microscope due to the small degree of circular polarization produced by a magnetic sample as well as the relatively low intensity of the emitted light.⁴ The light intensity is low despite the fact that the electric field at the tip of an STM can be strongly enhanced by interface plasmons localized between the sharp tip apex and the substrate. Without the enhancement the light intensity would be smaller by several orders of magnitude. Other techniques to develop magnetic microscopes based on apertureless near-field scanning have resolution on the order of at least 100 nm.⁶⁻⁸ Attempts to measure magnetic surface structure by means of the STM tunneling current⁹ have also been made and recently the

magnetic structure of an antiferromagnetic overlayer was mapped using this technique.¹⁰

In the scheme we propose, the scattered laser light intensity is large compared to that produced in STM light emission experiments making detection far easier. The circular polarization of the scattered light has both a component that is independent of the state of magnetization of the sample and a component that depends on the magnetization. The latter effect is rather small both when light is scattered from a magnetic surface as in the surface magneto-optic Kerr effect, and when light is emitted from an STM. However, when a tip is present and a laser provides incident light that is linearly polarized parallel to the surface (s polarized) and propagating in the direction of magnetization, we find up to two orders of magnitude increase in the degree of circular polarization compared with the basic Kerr effect which is generally of order 0.1 %. This enhancement occurs because the s polarized light that scatters from the tip and substrate develops a component in the direction perpendicular to the surface that is out of phase with the s polarized light. This is due to (1) the ordinary Kerr effect in which some of the incoming s polarized light is converted to p polarization and (2) the Kerr effect that acts on the light that is scattered between the tip and the substrate in the near field. The components of these fields that are perpendicular to the surface and lie between the tip and sample are enhanced by one to two orders of magnitude with a corresponding increase in the circular polarization.

The part of the circular polarization that does not depend on the magnetism of the surface is due to light that is reflected from both the tip and sample surface. The

surface reflection coefficients for s polarized and p polarized light result in phase differences that produce circular polarized light. This circular polarization is large and has a characteristic dependence on the observation angle which is different from the one displayed by the circular polarization that is due to magnetic effects. This difference in angular dependence may help in separating the two contributions.

The resolution of the microscope is roughly set by the radius of the tip (probe). A smaller probe gives a better resolution, however, one must also take into account that a very small probe gives a very small scattering cross section. At the same time, we find that a small probe is essential in obtaining a high degree of magnetism-dependent polarization of the scattered light. Our results indicate that a probe size of about 20 nm is optimal in striking the balance between these conflicting requirements.

The paper is organized in the following way. In section II we present a general theory with which we can solve the multiple-scattering problem defined by the model tip-sample geometry and calculate the scattered radiation and its polarization state. This theory uses a spherical model tip. The electromagnetic field is calculated taking retardation effects fully into account, while the magneto-optic corrections to the reflection coefficients of the sample are treated to first order in the off-diagonal elements of the dielectric tensor. In section III, we discuss the limit of a point dipole tip, in order to demonstrate the central physics more clearly, and also to make a comparison with the case of light emission from an STM probing a magnetic surface.⁵ In Sec. IV we present and discuss the numerical results obtained using the general theory of Sec. II.

II. THEORY

A. Basic considerations

In this section we present a theoretical formalism that allows us to calculate the polarization of light scattered from a tip-sample geometry in which the model tip is a sphere of finite size (the radius of the sphere corresponds roughly to the radius of curvature of the real tip). The calculation takes into account higher multipoles on the sphere as well as retardation effects.

We consider a situation illustrated in Fig. 1 where the magnetic sample fills the half-space $z > 0$, the model tip is a sphere with radius R that has its center on the z axis at $z = -(d+R)$, thus the tip-sample separation (smallest distance) is d . A plane wave incident on this system with wave vector \mathbf{q} can be written as (all fields etc. vary with time as $e^{-i\omega t}$, but we omit this factor here and in the following)

$$\mathbf{E}(\mathbf{r}) = \left\{ E^{(s)}[\hat{\mathbf{z}} \times \hat{\mathbf{q}}_{\parallel}] - E^{(p)}[\hat{\mathbf{q}} \times (\hat{\mathbf{z}} \times \hat{\mathbf{q}}_{\parallel})] \right\} e^{i\mathbf{q} \cdot \mathbf{r}}. \quad (2.1)$$

For any given wave vector \mathbf{q} the polarization vectors for s and p polarization are, respectively,

$$\hat{\mathbf{s}} = \hat{\mathbf{z}} \times \hat{\mathbf{q}}_{\parallel}$$

and

$$\hat{\mathbf{p}} = -\hat{\mathbf{q}} \times (\hat{\mathbf{z}} \times \hat{\mathbf{q}}_{\parallel}),$$

where \mathbf{q}_{\parallel} is the projection of \mathbf{q} in the surface plane. Both $\hat{\mathbf{s}}$ and $\hat{\mathbf{p}}$ are orthogonal to the unit vector $\hat{\mathbf{q}}$. We will calculate the radiation sent out in an arbitrary direction $\hat{\mathbf{q}}'$ after reflection off the tip-sample system. The radiated electric field propagating along $\hat{\mathbf{q}}'$ can be written as

$$\mathbf{E}_{\text{rad}} = \left\{ E_{\text{rad}}^{(s)}[\hat{\mathbf{z}} \times \hat{\mathbf{q}}'_{\parallel}] - E_{\text{rad}}^{(p)}[\hat{\mathbf{q}}' \times (\hat{\mathbf{z}} \times \hat{\mathbf{q}}'_{\parallel})] \right\} e^{i\mathbf{q}' \cdot \mathbf{r}}. \quad (2.2)$$

The polarization state of this radiation is different from that of the incoming light. First, there is a rather large, in this context less interesting, contribution to the circular polarization that comes about because the reflection probability from the surface is different for s polarized and p polarized light. In addition, the scattered light acquires a certain degree of circular polarization due to the Kerr effect; of course, for our purposes this is the interesting contribution. An incident s polarized wave will electrically polarize the tip in a direction parallel to the sample surface, but reflections off the magnetic sample surface also gives rise to a field component perpendicular to the surface. There is a strong enhancement of the component of the field perpendicular to the surface due to the cavity formed between tip and sample, and therefore this second contribution to the circular polarization should also be detectable.

The degree of circular polarization of the outgoing radiation is given in terms of the Stokes parameters as

$$\rho_{\text{CP}} = \frac{S_3}{S_0}. \quad (2.3)$$

Following Jackson's definitions,¹¹ the Stokes parameter S_0 is proportional to the total radiated differential power, whereas S_3 is proportional to the difference in intensity between left and right hand circularly polarized light. With the geometry illustrated in Fig. 1, one finds that in the radiation zone, far away from the tip and the sample surface, $\hat{\mathbf{s}} = \hat{\phi}'$ and $\hat{\mathbf{p}} = \hat{\theta}'$, where $\hat{\phi}'$ and $\hat{\theta}'$ denote the angular direction of the scattered light.

Left hand circularly polarized light (positive helicity) is associated with the unit polarization vector $\hat{\epsilon}_+ = (\hat{\mathbf{p}} + i\hat{\mathbf{s}})/\sqrt{2}$, while for right hand circularly polarized light (negative helicity) $\hat{\epsilon}_- = (\hat{\mathbf{p}} - i\hat{\mathbf{s}})/\sqrt{2}$. For the radiation propagating along the $\hat{\mathbf{q}}'$ -direction

$$S_0 \equiv |\hat{\epsilon}_+^* \cdot \mathbf{E}_{\text{rad}}|^2 + |\hat{\epsilon}_-^* \cdot \mathbf{E}_{\text{rad}}|^2 = |E_{\text{rad}}^{(p)}|^2 + |E_{\text{rad}}^{(s)}|^2, \quad (2.4)$$

and

$$S_3 \equiv |\hat{\epsilon}_+^* \cdot \mathbf{E}_{rad}|^2 - |\hat{\epsilon}_-^* \cdot \mathbf{E}_{rad}|^2 = -2 \operatorname{Im} \left[E_{rad}^{(s)*} E_{rad}^{(p)} \right]. \quad (2.5)$$

Hence the degree of polarization can be expressed as

$$\rho_{CP} = -2 \operatorname{Im} \left[\frac{E_{rad}^{(s)*} E_{rad}^{(p)}}{|E_{rad}^{(p)}|^2 + |E_{rad}^{(s)}|^2} \right]. \quad (2.6)$$

B. Sample dielectric tensor

We have expressed the measured magnetic circular dichroism in terms of the field amplitudes at the detector. These in turn have to be calculated with the tip-sample geometry and tip and sample dielectric functions as input.¹² Because the sample is magnetic, its dielectric function is a matrix that takes the form

$$\epsilon_{ij} = \begin{pmatrix} \epsilon_S(\omega) & \epsilon_1 \cos \varphi & -\epsilon_1 \sin \gamma \sin \varphi \\ -\epsilon_1 \cos \varphi & \epsilon_S(\omega) & \epsilon_1 \cos \gamma \sin \varphi \\ \epsilon_1 \sin \gamma \sin \varphi & -\epsilon_1 \cos \gamma \sin \varphi & \epsilon_S(\omega) \end{pmatrix} \quad (2.7)$$

where $\epsilon_S(\omega)$ is the substrate dielectric function. (Sometimes ϵ_1 appearing in the off-diagonal elements is written $\epsilon_1(\omega) \equiv iQ(\omega)\epsilon_S(\omega)$, Q being the so called magneto-optical constant.) The angles φ and γ relative to the x axis specify the direction of the magnetization. We will work in a configuration where $\varphi = \gamma = \pi/2$ which means that the magnetization is directed along the y -axis

$$\mathbf{M} = M\hat{\mathbf{M}} = M\hat{\mathbf{y}},$$

(see Fig. 1). Then the dielectric tensor for the sample takes the form¹³

$$\epsilon_{ij} = \begin{pmatrix} \epsilon_S(\omega) & 0 & -\epsilon_1(\omega) \\ 0 & \epsilon_S(\omega) & 0 \\ \epsilon_1(\omega) & 0 & \epsilon_S(\omega) \end{pmatrix}. \quad (2.8)$$

In Table I we list values, taken from Ref. 14, for $\epsilon_1(\omega)$ used in the present calculations.

C. Surface response

When a plane wave of the form in Eq. (2.1) is reflected from the sample surface, \mathbf{q}_{\parallel} remains unchanged. The reflected wave can in general be written as

$$\mathbf{E}_r = \left\{ E_r^{(s)} [\hat{\mathbf{z}} \times \hat{\mathbf{q}}_{\parallel}] - E_r^{(p)} [\hat{\mathbf{q}} \times (\hat{\mathbf{z}} \times \hat{\mathbf{q}}_{\parallel})] \right\} e^{i\mathbf{q}_- \cdot \mathbf{r}}, \quad (2.9)$$

where

$$\mathbf{q}_- = (\mathbf{q}_{\parallel}, -p) \quad \text{with} \quad p = \sqrt{k^2 - q_{\parallel}^2}$$

and $k = \omega/c$, the subscript $-$ expressing that the reflected wave propagates in the negative z direction.

The reflected amplitude varies linearly with the amplitudes of the incident wave. Thus, for s polarization,

$$E_r^s = \rho_s E^{(s)} + \rho'_{sp} E^{(p)}. \quad (2.10)$$

The response function ρ_s describes the ‘‘normal’’ reflection that takes place whether or not the sample is magnetic. The Fresnel formula for s polarization is

$$\rho_s = \frac{p - p_S}{p + p_S}, \quad (2.11)$$

where

$$p_S = \sqrt{k_S^2 - q_{\parallel}^2}.$$

$k = \omega/c$, and $k_S = k\sqrt{\epsilon_S(\omega)}$ are the wave-vector magnitudes in vacuum and the sample material, respectively. The second term in Eq. (2.10) applies to magnetic surfaces for which the off-diagonal element $\epsilon_1(\omega)$ in the dielectric tensor is non-zero and polarization mixing as a result of ‘‘anomalous’’ reflection events becomes possible. The conversion factor can be explicitly written as

$$\rho'_{sp} = \frac{\epsilon_1(\omega) q_{\parallel} p k}{p_S (p + p_S) (\epsilon_S(\omega) p + p_S)} [\hat{\mathbf{M}} \cdot \hat{\mathbf{q}}_{\parallel}] \equiv \rho_L [\hat{\mathbf{M}} \cdot \hat{\mathbf{q}}_{\parallel}]. \quad (2.12)$$

This expression can be derived by the methods developed by Zak *et al.*¹³ There is also a contribution from the off-diagonal elements in the dielectric tensor to the s -to- s reflection coefficient. However, this contribution is exceedingly small since it depends on the square of $\epsilon_1(\omega)$ and we neglect it in the following.

In analogy with Eq. (2.10), the reflected p polarized light is associated with the electric field

$$E_r^p = \rho_p E^{(p)} + \rho'_{ps} E^{(s)} + \rho'_{pp} E^{(p)}. \quad (2.13)$$

In this case the Fresnel formula is

$$\rho_p = \frac{\epsilon_S(\omega) p - p_S}{\epsilon_S(\omega) p + p_S}, \quad (2.14)$$

while the conversion factors originating from $\epsilon_1(\omega)$, ρ'_{ps} and ρ'_{pp} are given by

$$\rho'_{ps} = -\rho'_{sp} = -\rho_L [\hat{\mathbf{M}} \cdot \hat{\mathbf{q}}_{\parallel}], \quad (2.15)$$

[ρ_L was introduced in Eq. (2.12)] and

$$\rho'_{pp} = \frac{2\epsilon_1(\omega) p q_{\parallel}}{(\epsilon_S(\omega) p + p_S)^2} [\hat{\mathbf{z}} \cdot (\hat{\mathbf{q}}_{\parallel} \times \hat{\mathbf{M}})] \equiv \rho_T [\hat{\mathbf{z}} \cdot (\hat{\mathbf{q}}_{\parallel} \times \hat{\mathbf{M}})]. \quad (2.16)$$

Thus, unlike ρ'_{ps} and ρ'_{sp} , ρ'_{pp} vanishes when \mathbf{q}_{\parallel} and \mathbf{M} are parallel. Figure 2 illustrates the three possible anomalous scattering processes.

The expressions for all the surface response functions can be extended to the case of evanescent waves for which $q_{\parallel} = |\mathbf{q}_{\parallel}| > k$, and p is imaginary. (When evaluating the square roots defining p and p_S the branch cut lies below the positive real axis.) Later when we deal with the coupling between the sphere and the sample this becomes important since the coupling is mediated both by propagating and evanescent waves.

D. Scattering from the sphere

We now deal with the scattering off a sphere whose optical properties are described by its dielectric function $\epsilon_T(\omega)$. To this end we expand the electromagnetic field inside, and just outside the sphere in terms of electric (E) and magnetic (M) multipoles. We use the same notation as Jackson,¹¹ so that inside the sphere the electric field is written (the spherical coordinate system used here has the origin at the center of the sphere)

$$\mathbf{E} = \sum_{lm} k c_{lm}^{(M)} j_l(k_T r) \mathbf{X}_{lm} + \frac{i}{\epsilon_T} \nabla \times \left[c_{lm}^{(E)} j_l(k_T r) \mathbf{X}_{lm} \right], \quad (2.17)$$

while just outside the sphere the solution is a linear combination of incident and outgoing waves which can be written

$$\mathbf{E} = \sum_{lm} k [a_{lm}^{(M)} j_l(kr) + b_{lm}^{(M)} h_l(kr)] \mathbf{X}_{lm} + i \nabla \times \left\{ [a_{lm}^{(E)} j_l(kr) + b_{lm}^{(E)} h_l(kr)] \mathbf{X}_{lm} \right\}. \quad (2.18)$$

The corresponding magnetic field outside the sphere is

$$\mathbf{B} = \sum_{lm} \frac{k}{c} [a_{lm}^{(E)} j_l(kr) + b_{lm}^{(E)} h_l(kr)] \mathbf{X}_{lm} - \frac{i}{c} \nabla \times \left\{ [a_{lm}^{(M)} j_l(kr) + b_{lm}^{(M)} h_l(kr)] \mathbf{X}_{lm} \right\}. \quad (2.19)$$

Here the vector spherical harmonics are defined as

$$\mathbf{X}_{lm}(\theta, \phi) \equiv [\mathbf{L} Y_{lm}(\theta, \phi)] / \sqrt{l(l+1)}, \quad (2.20)$$

$\mathbf{L} \equiv -i\mathbf{r} \times \nabla$ is the angular momentum operator, and Y_{lm} are the usual spherical harmonics. The vector spherical harmonics form an orthonormal set of functions on the surface of a unit sphere. The functions j_l denote spherical Bessel functions, while $h_l \equiv h_l^{(1)}$ are spherical Hankel functions describing outgoing waves. As before $k = \omega/c$, $k_T = \sqrt{\epsilon_T} k$, and r denotes the distance from the center of the sphere. The coefficients c_{lm} , a_{lm} , and b_{lm} for the different multipoles are as yet unknown; they will be calculated in the following.

Since the angular momentum operator \mathbf{L} does not have any vector component in the radial direction, the same

holds true for \mathbf{X}_{lm} . Consequently, for an electric multipole field, the magnetic field does not have a radial component. On the other hand the electric field, as one should expect by visualizing the field from an electric dipole, has a radial component. For a magnetic multipole field, the roles are interchanged; the magnetic field but not the electric field has a radial component.

In the present context, we are primarily interested in knowing how the sphere acts as a scatterer. It therefore suffices to know what outgoing waves are obtained for given incident waves. The ratio between the b and a coefficient for each multipole provides this information. By demanding that the tangential \mathbf{E} and \mathbf{H} fields and the normal \mathbf{B} and \mathbf{D} fields are continuous we arrive at the following expressions for the sphere “response” functions

$$s_l^{(E)} \equiv \frac{b_{lm}^{(E)}}{a_{lm}^{(E)}} = - \frac{\epsilon_T k R j_l'(kR) + j_l(kR) (\epsilon_T - 1 - \mathcal{J}_l)}{\epsilon_T k R h_l'(kR) + h_l(kR) (\epsilon_T - 1 - \mathcal{J}_l)}, \quad (2.21)$$

and

$$s_l^{(M)} \equiv \frac{b_{lm}^{(M)}}{a_{lm}^{(M)}} = - \frac{k R j_l'(kR) - j_l(kR) \mathcal{J}_l}{k R h_l'(kR) - h_l(kR) \mathcal{J}_l}, \quad (2.22)$$

where \mathcal{J}_l is shorthand for

$$\mathcal{J}_l = k_T R j_l'(k_T R) / j_l(k_T R).$$

Thanks to the symmetry of the sphere these response functions are independent of m .

One additional ingredient is needed before we can calculate the field around the sphere when it is interacting with the sample. We have to be able to calculate “overlap integrals” between plane waves and multipole fields and vice versa. (Note that for lack of a better terminology, we will use “plane wave” as a common name both for propagating plane waves and waves that propagate in the directions parallel to the sample surface but are evanescent in the third, z direction). A plane wave, like the one in Eq. (2.1), impinging on the sphere can be expanded in terms of regular multipole contributions [the j_l terms in Eqs. (2.18) and (2.19)]. The resulting a coefficients depend linearly on the amplitudes of the incoming wave

$$\begin{aligned} a_{lm}^{(E)} &= f_{lm}^{Ep}(\mathbf{q}) E^{(p)} + f_{lm}^{Es}(\mathbf{q}) E^{(s)}, \quad \text{and} \\ a_{lm}^{(M)} &= f_{lm}^{Mp}(\mathbf{q}) E^{(p)} + f_{lm}^{Ms}(\mathbf{q}) E^{(s)}. \end{aligned} \quad (2.23)$$

Explicit expressions for the proportionality factors f are derived in the Appendix.

We also have to go in the opposite direction, from a certain multipole to a plane wave. In general the field radiated from the sphere can be written as

$$\begin{aligned} \mathbf{E}(\mathbf{r}) &= \sum_{lm, \sigma} b_{lm}^{\sigma} \int \frac{d^2 Q_{\parallel}}{(2\pi)^2} e^{i\mathbf{Q} \cdot \mathbf{r}} \\ &\times \left[g_{lm}^{s\sigma}(\mathbf{Q})(\hat{\mathbf{z}} \times \hat{\mathbf{Q}}_{\parallel}) - g_{lm}^{p\sigma}(\mathbf{Q})(\hat{\mathbf{Q}} \times (\hat{\mathbf{z}} \times \hat{\mathbf{Q}}_{\parallel})) \right]. \end{aligned} \quad (2.24)$$

Here $\mathbf{Q} = \mathbf{Q}_{\parallel} \pm \hat{\mathbf{z}} \sqrt{k^2 - Q_{\parallel}^2}$ (the sign is chosen according to the direction of propagation or exponential decay relative to the z axis) and σ denotes a polarization [(E) or (M)]. The factors $g_{lm}^{s\sigma}(\mathbf{Q})$ and $g_{lm}^{p\sigma}(\mathbf{Q})$ are the contributions of a given multipole on the sphere, (l, m, σ) , to the amplitude of a plane wave with wave vector \mathbf{Q} . The explicit calculation of these factors is deferred to the Appendix.

E. Solution of the multiple-scattering problem

We are now in a position to solve the multiple-scattering problem by using the same method as in a previous paper.¹⁵ We solve for the fields at the surface of the sphere and then calculate the electromagnetic fields elsewhere, in particular the radiated fields found far from the tip and sample.

In order to carry out the calculations, it is convenient to collect the a and b coefficients of Eqs. (2.18) and (2.19) into vectors \vec{a} and \vec{b} (in ‘‘multipole space’’) with the structure

$$\vec{a} = \left(a_{1-1}^{(E)}; a_{10}^{(E)}; \dots; a_{l_{max}l_{max}}^{(E)}; a_{1-1}^{(M)}; \dots; a_{l_{max}l_{max}}^{(M)} \right), \quad (2.25)$$

and similarly for \vec{b} . At the same time a diagonal tensor $\overleftrightarrow{\mathbf{s}}$, can be formed from the sphere response functions in Eqs. (2.21) and (2.22), so that one can write

$$\vec{b} = \overleftrightarrow{\mathbf{s}} \vec{a}. \quad (2.26)$$

The magneto-optic surface response functions ρ'_{ps} , ρ'_{sp} , and ρ'_{pp} are small, and one can therefore treat the magneto-optic effects by means of a series expansion in ϵ_1 . We begin by calculating the fields to *zeroth order in the magneto-optic response*. The field impinging on the sphere is a sum of three contributions (Figure 3) which in our vector notation can be written

$$\vec{a} = \vec{a}^{\text{dir}} + \vec{a}^{\text{ref}} + \overleftrightarrow{\mathbf{N}} \vec{a}. \quad (2.27)$$

Here \vec{a}^{dir} represents the amplitude of the field from the original incident wave; \vec{a}^{ref} gives the amplitude from the incident wave reflected *once* from the sample; and finally, $\overleftrightarrow{\mathbf{N}} \vec{a}$ represent waves sent out from the sphere itself that return to it after being reflected from the sample. Note that since the last term contains the exact field (\vec{a}) it accounts for all multiple scattering events in which light is scattered between the sphere and sample an arbitrary number of times.

With an incident wave given by Eq. (2.1), the elements entering \vec{a}^{dir} are found by using Eq. (2.23) together with Eqs. (A6) and (A7). In an analogous way, the elements of \vec{a}^{ref} are

$$\begin{aligned} a_{lm}^{(E),\text{ref}} &= f_{lm}^{Ep}(\mathbf{q}_-) \rho_p E^{(p)} + f_{lm}^{Es}(\mathbf{q}_-) \rho_s E^{(s)}, \quad \text{and} \\ a_{lm}^{(M),\text{ref}} &= f_{lm}^{Mp}(\mathbf{q}_-) \rho_p E^{(p)} + f_{lm}^{Ms}(\mathbf{q}_-) \rho_s E^{(s)}. \end{aligned} \quad (2.28)$$

Here $\rho_p E^{(p)}$ and $\rho_s E^{(s)}$ are the amplitudes of the reflected wave. The f functions now have \mathbf{q}_- as an argument since the direction of propagation relative to the z axis changes upon reflection. In the last term of Eq. (2.27), $\overleftrightarrow{\mathbf{N}}$ is a tensor in multipole space. Its elements describe how a wave with angular momentum l' and m' and polarization σ' hits the sphere, is reflected, and returns to the sphere again after reflection from the plane, now with angular momentum l and m and polarization σ . As a consequence, a tensor element is written

$$N_{lm,l'm'}^{\sigma\sigma'} = s_{l'}^{\sigma'} \int \frac{d^2 Q_{\parallel}}{(2\pi)^2} \sum_{\sigma''} f_{lm}^{\sigma\sigma''}(\mathbf{Q}_-) \rho_{\sigma''}(Q_{\parallel}) g_{l'm'}^{\sigma''\sigma'}(\mathbf{Q}_+). \quad (2.29)$$

In this equation σ'' stands for either s or p polarization, and

$$\mathbf{Q}_{\pm} = \mathbf{Q}_{\parallel} \pm \hat{\mathbf{z}} \sqrt{k^2 - |\mathbf{Q}_{\parallel}|^2}.$$

Equation (2.29) can be derived formally along the lines of the calculation presented in Ref. 15, but it can also be understood in a more intuitive way as follows (see Fig. 3 for a schematic illustration). The first factor $s_{l'}^{\sigma'}$, connects the a coefficient of the initially incident multipole to the corresponding b coefficient; then the function $g(\mathbf{Q}_+)$ describes the overlap between the multipole l', m', σ' and a plane wave, ρ the reflection of that plane wave off the sample, and $f(\mathbf{Q}_-)$ gives the overlap between the reflected wave and the multipole l, m, σ . Because the propagation to the sample surface and back involves all wave vectors, a two-dimensional wave-vector integration is required. To evaluate Eq. (2.29) it is best to use cylindrical coordinates in which the angular integration is trivial. Thanks to the cylindrical symmetry of the model geometry only tensor elements with $m = m'$ are non-zero. The remaining $|\mathbf{Q}_{\parallel}|$ integration runs from 0 to ∞ so that the sphere-sample coupling is mediated by both propagating and evanescent waves.

Equation (2.27) is solved by a matrix inversion (of course then only a finite number of multipoles can be retained)

$$\vec{a} = \left[\overleftrightarrow{\mathbf{1}} - \overleftrightarrow{\mathbf{N}} \right]^{-1} (\vec{a}^{\text{dir}} + \vec{a}^{\text{ref}}). \quad (2.30)$$

Knowing the coefficients a_{lm} we can calculate the electromagnetic field everywhere to zeroth order in the magneto-optic response. The various ingredients entering the calculation of the scattering processes are shown schematically in Fig. 3.

We next proceed to calculate the corrections to the fields to *first order in the magneto-optic response*. To this end we introduce another set of coefficients $a_{lm}^{(E)}$ and $a_{lm}^{(M)}$ that vary linearly with ϵ_1 , the off-diagonal elements

of the sample dielectric tensor. Together $a_{lm}^{(E)}$ and $a_{lm}^{(M)}$ form the vector \vec{a}' in multipole space. One can solve for \vec{a}' from the equation

$$\vec{a}' = \vec{a}'^{\text{ext}} + \overleftrightarrow{N}\vec{a}', \quad (2.31)$$

in which all terms are first order in ϵ_1 . The first term on the right hand side acts as a source term for the first-order-in- ϵ_1 fields, while the last term accounts for multiple, normal (i.e. not involving the Kerr effect) reflections between the tip and sample; the fields appearing there, described by \vec{a}' , have already undergone an anomalous reflection.

There are two contributions to \vec{a}'^{ext} , one due to an anomalous reflection of the incident wave the very first time it hits the sample, and one due to waves incident from the sphere that are anomalously reflected, thus

$$\vec{a}'^{\text{ext}} = \vec{a}'^{\text{ref}} + \overleftrightarrow{K}\vec{a}'. \quad (2.32)$$

Both terms on the right hand side are first order in ϵ_1 , the first one being the ordinary Kerr term and the second the tip-induced Kerr term. In analogy with Eq. (2.28),

$$\begin{aligned} a_{lm}^{(E),\text{ref}} &= f_{lm}^{Ep}(\mathbf{q}_-)(\rho'_{pp}E^{(p)} + \rho'_{ps}E^{(s)}) \\ &+ f_{lm}^{Es}(\mathbf{q}_-)\rho'_{sp}E^{(p)} \end{aligned} \quad (2.33)$$

and

$$\begin{aligned} a_{lm}^{(M),\text{ref}} &= f_{lm}^{Mp}(\mathbf{q}_-)(\rho'_{pp}E^{(p)} + \rho'_{ps}E^{(s)}) \\ &+ f_{lm}^{Ms}(\mathbf{q}_-)\rho'_{sp}E^{(p)}. \end{aligned} \quad (2.34)$$

In these expressions we have suppressed the \mathbf{q}_{\parallel} dependence of ρ'_{pp} , ρ'_{ps} , and ρ'_{sp} . This dependence becomes important when evaluating the tensor elements in \overleftrightarrow{K} ,

$$\begin{aligned} K_{lm,l'm'}^{\sigma\sigma'} &= s_{l'}^{\sigma'} \sum_{\sigma'',\sigma'''} \\ &\times \int \frac{d^2Q_{\parallel}}{(2\pi)^2} f_{lm}^{\sigma\sigma''}(\mathbf{Q}_-)\rho'_{\sigma'',\sigma'''}(\mathbf{Q}_{\parallel})g_{l'm'}^{\sigma'''\sigma'}(\mathbf{Q}_+). \end{aligned} \quad (2.35)$$

Here σ'' and σ''' stand for either s or p polarization (and $\rho'_{ss} = 0$ to first order in ϵ_1). The various factors play the same roles here as in Eq. (2.29) except, of course, for the fact that we now collect the effects of anomalous reflection events in the sample described by $\rho'_{\sigma''\sigma''}$. As in the previous case the angular integrations can be done analytically, and here, due to the angular dependence of $\rho'_{\sigma,\sigma'}$, an element in \overleftrightarrow{K} is nonzero if, and only if, $m = m' \pm 1$. Once \overleftrightarrow{K} has been calculated, we evaluate \vec{a}'^{ext} and then solve for \vec{a}'

$$\vec{a}' = \left[\overleftrightarrow{1} - \overleftrightarrow{N} \right]^{-1} \vec{a}'^{\text{ext}} = \left[\overleftrightarrow{1} - \overleftrightarrow{N} \right]^{-1} \left[\vec{a}'^{\text{ref}} + \overleftrightarrow{K}\vec{a}' \right]. \quad (2.36)$$

F. Radiated field

Finally, we calculate the radiated fields, and the degree of polarization. To this end we add together all contributions to the radiated field that have scattered from the sphere at one time or another.

To zeroth order in ϵ_1 , the field is found by considering the outgoing waves coming from the sphere as well as the corresponding waves reflected (normal reflection) off the sample surface. The specularly reflected wave that has not interacted with the sphere is ignored since an experimental measurement that is sensitive to polarization changes induced by the Kerr effect must avoid this otherwise dominating, direct contribution.

The radiated field is calculated to first order in ϵ_1 along the same lines using the a_{lm}' terms instead of the a_{lm} terms in the multipole expansion as a source for the radiation. There is also an additional, in practice rather small, contribution to the first-order fields that results from anomalous reflection of zeroth-order waves coming from the sphere and scattering off the sample surface a last time before going out to infinity.

The field radiated directly from the sphere into a direction defined by the angles θ' and ϕ' [$(\theta', \phi') \equiv \Omega'$] can be calculated by means of a stationary phase approximation yielding

$$\begin{aligned} \mathbf{E}_{\text{dir}} &= -\frac{e^{ikr}}{r} \frac{ik \cos \theta'}{2\pi} \sum_{lm\sigma} s_l^{\sigma} a_{lm}^{\Sigma,\sigma} \\ &\times \left[\hat{\theta}' g_{lm}^{p\sigma}(\mathbf{q}'_-) + \hat{\phi}' g_{lm}^{s\sigma}(\mathbf{q}'_-) \right]. \end{aligned} \quad (2.37)$$

Here

$$\mathbf{q}'_- = k\hat{\mathbf{q}}_- = k \sin \theta' (\hat{\mathbf{x}} \cos \phi' + \hat{\mathbf{y}} \sin \phi') - k|\cos \theta'| \hat{\mathbf{z}}.$$

(with an analogous definition, having a positive z component, for \mathbf{q}'_+ used below), and

$$a_{lm}^{\Sigma,(M)} = a_{lm}^{(M)} + a_{lm}'^{(M)}, \quad \text{and} \quad a_{lm}^{\Sigma,(E)} = a_{lm}^{(E)} + a_{lm}'^{(E)},$$

so that the expression contains contributions to both zeroth and first order in ϵ_1 . The radiation resulting from normal or anomalous reflections from the sample surface can be calculated in a way analogous to Eq. (2.37). The only modifications are that one must (i) multiply by the appropriate reflection factor, and (ii) use \mathbf{q}'_+ instead of \mathbf{q}'_- as an argument in g since the light in this case first propagates towards the sample after having left the sphere.

These contributions can now be added together so that the polarization ρ_{CP} , of the outgoing light that has been scattered off the sphere at least once can be calculated. We obtain¹⁶

$$\begin{aligned} E_{\text{rad}}^{(s)} &= -\frac{e^{ikr}}{r} \frac{ik \cos \theta'}{2\pi} \sum_{lm\sigma} s_l^{\sigma} a_{lm}^{\Sigma,\sigma} \\ &\times \left[g_{lm}^{s\sigma}(\mathbf{q}'_-) + \rho_s(k \sin \theta') g_{lm}^{s\sigma}(\mathbf{q}'_+) \right. \\ &\left. + \sin \phi' \rho'_{sp}(\mathbf{q}'_{\parallel}) g_{lm}^{p\sigma}(\mathbf{q}'_+) \right] \end{aligned} \quad (2.38)$$

and

$$E_{\text{rad}}^{(p)} = -\frac{e^{ikr}}{r} \frac{ik \cos \theta'}{2\pi} \sum_{lm\sigma} s_l^\sigma a_{lm}^{\Sigma, \sigma} \times [g_{lm}^{p\sigma}(\mathbf{q}'_-) + \rho_p(k \sin \theta') g_{lm}^{p\sigma}(\mathbf{q}'_+) + \cos \phi' \rho'_{pp}(\mathbf{q}'_{\parallel}) g_{lm}^{p\sigma}(\mathbf{q}'_+) + \sin \phi' \rho'_{ps}(\mathbf{q}'_{\parallel}) g_{lm}^{s\sigma}(\mathbf{q}'_+)], \quad (2.39)$$

where the terms are organized according to where the last scattering event takes place. The first terms describe waves that come directly from the sphere, the second terms give the contributions from waves that come from a final, normal scattering event from the sample, while the remaining terms originate from a final anomalous scattering event from the sample. The degree of circular polarization is then found by inserting these expressions into Eq. (2.6).

III. DIPOLE LIMIT

For illustrative purposes it is useful to study the theory developed in the previous section in a limit where both the sphere radius and the sphere-sample distance are much smaller than the wavelength of light. When these conditions are fulfilled the sphere can be treated as a point dipole and retardation effects are negligible.

Returning to Eqs. (2.21) and (2.22) we find the following limiting behavior for the sphere response functions when both $kR \ll 1$ and $|k_T R| \ll 1$,

$$s_l^{(E)} = \frac{i(kR)^{2l+1}(l+1)}{(2l-1)!!(2l+1)!!} \frac{\epsilon_T - 1}{l\epsilon_T + (l+1)}, \quad (3.1)$$

and

$$s_l^{(M)} = -\frac{i(kR)^{2l+3}}{(2l+1)!!(2l+3)!!}. \quad (3.2)$$

Thus the behavior of a small sphere is dominated by its electric-dipole response $s_1^{(E)} \sim R^3$. Therefore, in the rest of this section we will only discuss the electric dipole excitations of the sphere and the vectors \vec{a} and \vec{b} can effectively be reduced to just three components.

We also need limiting expressions for the coupling matrix elements $N_{10,10}^{EE}$, $N_{11,11}^{EE}$, and $N_{1-1,1-1}^{EE}$ (the other remaining elements of \overleftrightarrow{N} vanish). An explicit evaluation of $N_{11,11}^{EE}$ in which the large \mathbf{q}_{\parallel} limits of $\rho_p = (\epsilon_S - 1)/(\epsilon_S + 1)$, $\rho_s \rightarrow 0$, as well as f and g are used yields

$$N_{\parallel} \equiv N_{11,11}^{EE} = N_{1-1,1-1}^{EE} = \frac{\epsilon_T - 1}{\epsilon_T + 2} \frac{\epsilon_S - 1}{\epsilon_S + 1} \frac{R^3}{8(d+R)^3}. \quad (3.3)$$

This expression can be obtained from more intuitive reasoning. If an electric field $\mathbf{E} = E\hat{\mathbf{x}}$ polarizes the sphere, a dipole moment

$$\mathbf{p} = 4\pi\epsilon_0 R^3 \frac{\epsilon_T - 1}{\epsilon_T + 2} E\hat{\mathbf{x}} \quad (3.4)$$

is induced on the sphere, and there is an accompanying image dipole in the sample

$$\mathbf{p}_{\text{im}} = -\mathbf{p} \frac{\epsilon_S - 1}{\epsilon_S + 1}. \quad (3.5)$$

The electric field created by the image dipole at the center of the sphere is

$$\mathbf{E}_{\text{ind}} = \frac{\epsilon_T - 1}{\epsilon_T + 2} \frac{\epsilon_S - 1}{\epsilon_S + 1} \frac{R^3}{8(d+R)^3} \mathbf{E} \equiv N_{\parallel} \mathbf{E}. \quad (3.6)$$

This is just the way the matrix elements of N should work; given an incoming field at the sphere, N generates the fields reflected from the sphere and scattered back to it by the sample.

If the incident \mathbf{E} field points in the z direction the field from the image dipole, which now is proportional to $N_{10,10}^{EE}$ is twice as strong as in the previous, parallel case. Consequently we have,

$$N_{\perp} \equiv N_{10,10}^{EE} = \frac{\epsilon_T - 1}{\epsilon_T + 2} \frac{\epsilon_S - 1}{\epsilon_S + 1} \frac{R^3}{4(d+R)^3}. \quad (3.7)$$

One can also evaluate the K integrals describing the coupling due to magneto-optic effects. The results can be written

$$K \equiv K_{10,11}^{EE} = -K_{11,10}^{EE} = -K_{10,1-1}^{EE} = K_{1-1,10}^{EE} = \sqrt{2} \frac{\epsilon_T - 1}{\epsilon_T + 2} \frac{\epsilon_1}{(\epsilon_S + 1)^2} \frac{R^3}{8(d+R)^3}. \quad (3.8)$$

The other elements of \overleftrightarrow{K} vanish in this case.

If an s polarized wave with wave vector \mathbf{q} impinges on the system the wave incident on the dipole can be written

$$\vec{a}^{\text{dir}} + \vec{a}^{\text{ref}} = -2\pi i \sqrt{\frac{3}{4\pi}} [1 + \rho_s(\mathbf{q}_{\parallel})] \frac{E^{(s)}}{k} \begin{bmatrix} e^{i\phi} \\ 0 \\ e^{-i\phi} \end{bmatrix}, \quad (3.9)$$

where ϕ denotes the azimuthal angle of \mathbf{q} , the wave vector of the incident light. Because \overleftrightarrow{N} is diagonal it is simple to solve for the full vector \vec{a} using Eq. (2.30),

$$\vec{a} = -\frac{2\pi i}{1 - N_{\parallel}} \sqrt{\frac{3}{4\pi}} [1 + \rho_s(\mathbf{q}_{\parallel})] \frac{E^{(s)}}{k} \begin{bmatrix} e^{i\phi} \\ 0 \\ e^{-i\phi} \end{bmatrix}. \quad (3.10)$$

The sphere is only polarized parallel to the surface at this stage ($a_{10}^{(E)} = 0$).

Before proceeding further, let us insert the above result for \vec{a} into Eqs. (2.38) and (2.39) and calculate the polarization of the light sent out. Since $E_{\text{rad}}^{(s)}$ and $E_{\text{rad}}^{(p)}$ have many factors in common the final result can be written

$$\rho_{\text{CP}} = -2 \text{Im} \left[\frac{S^* P}{|S|^2 + |P|^2} \right], \quad (3.11)$$

where

$$\begin{aligned} S &= \cos(\phi' - \phi) \left[1 + \rho_s(q_{\parallel}') \right], \quad \text{and} \\ P &= \sin(\phi' - \phi) \left[1 - \rho_p(q_{\parallel}') \right] \cos \theta'. \end{aligned} \quad (3.12)$$

With appropriate parameter values Eq. (3.11) predicts a rather large circular polarization even if the sample is non-magnetic. If ρ_{CP} given by this expression is plotted as a function of ϕ' one typically obtains an oscillating curve. We also note that in this limit, ϕ' and $\phi' + \pi$ yields exactly the same ρ_{CP} . Thus, if we introduce the quantity

$$\Delta\rho_{\text{CP}}(\phi') = \rho_{\text{CP}}(\phi') - \rho_{\text{CP}}(\phi' + \pi), \quad (3.13)$$

we find that in the dipole limit, without a Kerr effect, $\Delta\rho_{\text{CP}} = 0$. This is an important observation since we will see that when the sample is magnetic this symmetry is lost.

Due to ϵ_1 , there are two contributions to \vec{a}'^{ext} ; the ordinary Kerr effect upon reflection of the incident field yields \vec{a}'^{ref} ,

$$\vec{a}'^{\text{ref}} = -\epsilon_1 \frac{q_{\parallel} p 2\pi \sqrt{3/4\pi} \sin \phi}{p_S(p + p_S)(\epsilon_S p + p_S)} \begin{bmatrix} -e^{i\phi} \cos \theta' \\ \sqrt{2} \sin \theta' \\ e^{-i\phi} \cos \theta' \end{bmatrix} E^{(s)}, \quad (3.14)$$

and the tip Kerr effect yields

$$\overleftrightarrow{K} \vec{a} = -\frac{4\pi K \sin \phi}{1 - N_{\parallel}} \sqrt{\frac{3}{4\pi}} [1 + \rho_s(q_{\parallel})] \frac{E^{(s)}}{k} \begin{bmatrix} 0 \\ 1 \\ 0 \end{bmatrix}. \quad (3.15)$$

Both contributions are first order in ϵ_1 , both have a $\sin \phi$ dependence on the direction of propagation of the incident light, and the Kerr effect induces a dipole moment perpendicular to the sample surface. We also see that resonances in the tip-sample interaction described by the factor $1/(1 - N_{\parallel})$ can enhance the tip Kerr effect (though for a point dipole model for the tip these effects are usually small).

We can now solve for \vec{a}' by making use of

$$\vec{a}' = \left(\overleftrightarrow{1} - \overleftrightarrow{N} \right)^{-1} \left(\vec{a}'^{\text{ref}} + \overleftrightarrow{K} \vec{a} \right), \quad (3.16)$$

where further tip-sample interactions are included. Next, inserting the sum $\vec{a}^{\Sigma} = \vec{a} + \vec{a}'$ into Eqs. (2.38) and (2.39), the polarization is found.

Before analyzing this it is illustrative to see what result we get for the magnetic contribution to the circular polarization, to lowest order in the ratio of $E_{\text{rad}}^{(p)}$ to $E_{\text{rad}}^{(s)}$, and comparing this to our earlier result in the reverse situation with light being emitted by tunneling electrons

instead.⁵ Inserting the dipolar results above for the ordinary and the tip Kerr effect into Eqs. (2.38) and (2.39) we obtain to lowest order, retaining only magnetic contributions to the circular polarization

$$\begin{aligned} \rho_{\text{CP}}^M &\approx \text{Im} \left[\frac{1 + G_{\perp}}{1 + G_{\parallel}} \left(\frac{-\rho_L(\omega)}{1 + \rho_s(q_{\parallel})} - \frac{D(\omega)G_{\parallel}}{\sin \theta'} \right) \frac{1 + \rho_p(q_{\parallel}')}{1 + \rho_s(q_{\parallel}')} \right] \\ &\times 2 \frac{\sin \phi \sin^2 \theta'}{\cos(\phi - \phi')}, \end{aligned} \quad (3.17)$$

where $\rho_L(\omega)$ is defined in Eq.(2.12) and¹⁷

$$D(\omega) = \frac{2\epsilon_1(\omega)}{\epsilon_S^2(\omega) - 1}. \quad (3.18)$$

Furthermore the image factors G are defined through

$$G_{\parallel, \perp} = N_{\parallel, \perp} / (1 - N_{\parallel, \perp}) \quad (3.19)$$

for the parallel and perpendicular cases, respectively. The result for the circular polarization of light in the corresponding spontaneous emission STM configuration is

$$\rho_{\text{CP}}^{\text{STM}} \approx 2 \text{Im} \left[\left(\frac{-\rho_L(\omega)}{1 + \rho_s} + \frac{D(\omega)G_{\parallel}}{\sin \theta'} \right) \frac{1 + \rho_s}{1 + \rho_p} \right]. \quad (3.20)$$

The structure is very similar to that of (3.17) but there are a couple of important differences. For the light-in situation the whole expression is basically larger by the factor G_{\perp} . This is one reason for why ρ_{CP}^M can be several orders of magnitude larger than $\rho_{\text{CP}}^{\text{STM}}$; the perpendicular field enhancement, G_{\perp} , can be very large in the junction between tip and sample, while G_{\parallel} is of order unity. Moreover, in the last factor $(1 + \rho_s)$ and $(1 + \rho_p)$ have changed places. This is also an important reason for the large values reached by ρ_{CP}^M . At a metal surface $(1 + \rho_s)$ is usually considerably smaller than 1.

Continuing the analysis of the full results we find that they can be summarized as

$$\vec{a} = \begin{bmatrix} (-ia_x + a_y)/\sqrt{2} \\ a_z \\ (ia_x + a_y)/\sqrt{2} \end{bmatrix}, \quad (3.21)$$

for \vec{a} , where a_x , a_y and a_z are proportional to the induced dipole moments in the x , y , and z directions, respectively. Let us assume from now on that the incident wave propagates in the negative y direction, so that $\phi = -\pi/2$. This means that a_x will be large, whereas a_y and a_z are much smaller since they originate from the Kerr effect. Therefore looking at the radiation sent out in two opposite directions (ϕ' and $\phi' + \pi$) we see that the contributions to $E_{\text{rad}}^{(p)}$ and $E_{\text{rad}}^{(s)}$ caused by the x and y components of the dipole moment both change sign upon changing the angle of observation, leaving the polarization state unchanged as we have already discussed. However, the new feature,

the dipole moment in the z direction adds the same contribution to $E_{\text{rad}}^{(p)}$ in both directions, thereby leading to an asymmetry in the angular dependence of the polarization. Anomalous reflection of the radiation sent out as a result of the dipole moment oscillating in the x direction also yields contributions to $E_{\text{rad}}^{(s)}$ and $E_{\text{rad}}^{(p)}$ that do not change sign when changing ϕ' to $\phi' + \pi$. From this follows that the magnetism-related contribution to the circular polarization has a characteristic angular dependence which, as we will see, persists also when going beyond the dipole model.

IV. RESULTS AND DISCUSSION

A. Numerical results

In this section we will present results of our numerical calculations. We have solved the multiple-scattering problem at hand using the theory developed in Sec. II. In these calculations we retained multipoles for which $l \leq 30$ and $|m| \leq 3$. This means that we get results that are essentially numerically exact; the relative accuracy obtained for $\Delta\rho_{\text{CP}}$ is better than 10^{-5} when $R = 20$ nm and $d = 0.5$ nm. If l_{max} is reduced to 10 the relative errors are about 1 %, and with $l_{\text{max}} = 5$ they amount to 5–10 %.

Figure 4 shows results for the polarization ρ_{CP} as a function of the observation angle ϕ' . These results were obtained from a calculation using a silver tip and an Fe sample. For comparison, we have also performed a calculation using a W tip [panel (c)]. The photon energy was 1.6 eV and both the incident and the scattered light propagates in directions forming an angle of 1 radian with the surface normal. This means that $\theta = 1$, while $\theta' = \pi - 1$.

Let us begin the discussion by looking at the results in Fig. 4 (a), where the Ag tip radius was set to 10 nm. Results are shown both with (thick curve) and without (thin curve) the magneto-optic effects; the two curves are very similar indicating that “geometric effects” cause the dominating contribution to the polarization ρ_{CP} . However, a closer comparison reveals that the results including magneto-optic effects show a less symmetric angular dependence than those obtained without taking magneto-optic effects into account. Therefore magneto-optic effects can be isolated more effectively if the quantity $\Delta\rho_{\text{CP}}$ defined in Eq. (3.13) is plotted. We see that $\Delta\rho_{\text{CP}}$ has peak values exceeding 10 %, and at the same time the polarization shows a simple, characteristic variation with the observation angle ϕ' . It appears that these effects are large enough to be detectable. We have also plotted the quantity $\delta\rho$, i.e. the change in ρ_{CP} due to magneto-optic effects. The two curves are very similar in shape.

In Fig. 4 (b) the tip radius was increased to 20 nm. The tip is now large enough that phase differences between light scattered off different parts of the tip influence the

polarization. This gives $\Delta\rho_{\text{CP}}$ a more complicated angular behavior, and it would be somewhat more difficult to pick out the part of the signal originating from the Kerr effect. For an even larger tip radius this effect becomes more pronounced.

There are two different magnetism-related processes that contribute to the circular polarization of the scattered light. We already mentioned this in connection with Eqs. (2.32) and (3.17), and the same distinction was also made in our previous work on light emission.⁵ To begin with there is an ordinary Kerr effect in which the polarization conversion, governed by the coefficient ρ'_{ps} , takes place primarily when the incident wave first hits the sample surface. This induced p polarized wave is subsequently enhanced in the cavity between tip and sample; both tip and sample screen the electric field, surface charges are induced on both of them and this generates secondary fields, etc. In the other process, which we have called the tip Kerr effect, the incident wave is reflected back and forth between tip and sample a number of times and an electric field along the z axis is built up because one of the scattering events off the sample is anomalous. In this case the anomalously reflected wave typically is evanescent since it describes the near field around the tip. The conversion factor ρ'_{pp} dominates these processes, because, as can be seen from Eqs. (2.12), (2.15), and (2.16), unlike ρ'_{ps} and ρ'_{sp} it has a non-zero limit when $q_{\parallel} \gg k$.

In the full (multipole) calculations the relative importance of the two processes can be estimated, for example, by temporarily eliminating one or the other contribution. We find that the ordinary Kerr effect in the present case is responsible for some two thirds of the magnetic contributions to the circular polarization of the scattered light. In the calculation addressing emission of circularly polarized light⁵ we found the opposite situation; the tip Kerr effect dominated then. It is relatively straightforward to understand this difference qualitatively: Near-field effects are considerably more important in the case of light emission because in that experiment one measures how much radiation is produced by a source, the tunnel current, that is basically localized to a nanometersized region in space. In the present calculation we instead probe the degree to which light is scattered off the tip-sample system; the near-field effects play a role also here but it is not as pronounced.

We have concentrated on studying the polarization properties of the scattered light at relatively low photon energies (< 2 eV) because ϵ_1 for the magnetic materials takes the largest values there. In that case the results obtained with a W tip (shown in panel c) and with a Ag tip (panel a) are not too different from each other. This result may at first seem surprising given that Ag is a much better conductor than W and has well-defined surface plasmon excitations. However, for the photon energies dealt with here the field enhancement does not occur as a result of truly *resonant* interactions with interface plasmons. Instead the electric field in the tip-sample cavity is

enhanced by a less dramatic mechanism. Both Ag and W screen the electric field and therefore surface charges that interact with each other are built up on the tip and sample. At higher photon energies a Ag tip certainly gives a stronger field enhancement than a W tip, but then again, since ϵ_1 for the magnetic materials is much lower there, this frequency range is of limited interest in the present context.

Figure 5 illustrates in more detail how the polarization properties of the scattered light varies with photon energy. The highest degree of polarization is reached at 1.5 eV. For photon energies beyond 2 eV the Kerr effect has a rather small influence on the polarization, the main reason for this is that the magnitude of ϵ_1 for Fe decreases with increasing $\hbar\omega$.

In Fig. 6 we plot the differential scattering cross section for a Ag tip with a radius of either 10 nm or 20 nm. As a reference we have also plotted the result obtained for a Ag sphere with radius 10 nm in free space. The sphere in front of an Fe sample has a much smaller cross section than the one in free space because of destructive interference between the waves sent out directly from the sphere and those reflected from the sample, which in this case can be thought of as originating primarily from an image sphere. The radiation patterns differ also between the two cases. An isolated sphere displays a dipole pattern, but with the sample present, the angular distribution of radiation mainly follows a quadrupole pattern. To see what the cross sections mean in terms of photon counts, let us assume that a laser with an intensity of 10^3 W/cm² is illuminating the tip. This is equivalent to a photon flow of $\sim 10^8$ photons/(sec. nm²). In the case of the 10-nm-sphere in front of the Fe sample, a detector covering a solid angle of 0.1 steradian would collect $\sim 10^3$ photons per second. This intensity should be enough to perform a polarization analysis.

B. Experimental implications

The measurement of the magnetic contribution to the circular polarization should be feasible in the sense that the scattered light intensity is sufficient and the degree of circular polarization of the scattered light is large enough to be detectable with existing optical techniques. Furthermore, it should at least be possible to reach a resolution of 10 nm. However, the removal of the background circular polarization which is not magnetic in origin is a nontrivial experimental problem. The Kerr contribution varies with scattering angle in a way which is different from other nonmagnetic contribution to the polarization, provided the tip is not too large. This should help in separating the two contributions to the circular polarization. It may also be possible to use the fact that the Kerr contribution to the circular polarization is more sensitive to the tip-sample distance than is the background circular polarization, for example by letting the tip vibrate back

and forth. To be specific, increasing the tip-sample distance from 0.5 nm to 5 nm in Fig. 4 (a) decreases the Kerr contribution ($\Delta\rho_{CP}$) by about a factor of 2, whereas the background contribution is essentially unchanged. Varying the photon energy could be yet another way of differentiating between Kerr and background contributions.

In view of the large background, the size of the tip would be a major concern in designing an experiment in practice. If a traditional STM tip made from a metallic wire is used, regardless of how sharp the tip is, scattering will take place everywhere in the tip shaft. This scattering will typically increase the geometric-background contribution to the circular polarization, and make it more difficult to detect the magnetic properties of the surface. Of course, the incident radiation would be focused to a relatively small part of the tip, but this may not be enough to obtain a high contrast between the contributions to the polarization induced by the Kerr effect and geometric effects, respectively.

As we have indicated in the Introduction, one possible way of bypassing this difficulty could be to follow a scheme closely related to that introduced by Silva and Schultz,⁶ using a small, isolated metallic particle on the surface of the magnetic sample as the probe. In order to scan different parts of the surface, the metallic particle would have to be moved around using an AFM. This kind of nanoparticle manipulation has already been achieved in other contexts.¹⁸

Pufall, Berger, and Schultz¹⁹ have measured the Kerr rotation of light scattered from Ag particles placed on a magnetic substrate. They found a Kerr rotation that had qualitative features (in terms of observation-angle dependence) in common with the results presented here. The measured Kerr rotation, however, was less than 1 mrad (corresponding to a magnetism-related degree of polarization of 0.1 % or less). It appears from Ref. 19 that particles of a radius of at least 50 nm were used in the experiment and at the same time the incident laser light was tuned to the scattering resonance of the particles at a wavelength of 460 nm (≈ 2.7 eV). While both of these choices ensure that the scattering cross section is much larger than with the parameter values used in the calculations above, this is achieved at the cost of a very small degree of magnetism-related polarization of the scattered light. First of all $\epsilon_1(\omega)$ in common magnetic metals such as Fe and Co decreases with increasing photon energy in the range of visible light (cf. Fig. 5). Secondly, with a larger particle the in-plane dipole becomes more effective in sending out radiation because the image sphere is further away from the real sphere. As a result the scattering cross section but also the nonmagnetic contributions to ρ_{CP} increase dramatically. Indeed, using a silver particle of radius $R = 50$ nm on a Fe substrate and a photon energy of 3 eV in our calculations we find that the magnetism-related contribution to the light polarization (i.e. $\delta\rho$) is only ≈ 0.1 %. With $R = 50$ nm and a photon energy of 1.6 eV, $\delta\rho \approx 2$ % at most, to be compared with 6–7 % for $R = 10$ nm (see Fig. 4 (a)). Thus, based on

the results found here we recommend that experiments of this kind should use smaller photon energies (1.5 eV or so) and smaller particles (~ 20 nm) than before.

ACKNOWLEDGMENTS

We would like to thank M. L. Cohen, R. J. Celotta, L. Montelius, and L. Samuelsson for useful discussions. SPA acknowledges a grant from Iberdrola S.A. The work of PJ and SPA is supported by the Swedish Natural Science Research Council, and by the European Union through TMR contract ERB-FMRX-0198.

APPENDIX:

In this Appendix, we derive expressions for the functions f and g that were introduced in Sec. IID. With a plane wave impinging on the sphere, the full electric field outside the sphere can be expanded as in Eq. (2.18), and the regular (j_l) terms describe the incoming wave. We will calculate the proportionality factors f appearing in Eq. (2.23), and therefore we first need to evaluate the a coefficients in Eq. (2.18). It is clear from Eq. (2.18), in view of the orthogonality relations

$$\int d\Omega \mathbf{X}_{l'm'}^*(\Omega) \cdot \mathbf{X}_{lm}(\Omega) = \delta_{ll'} \delta_{mm'} \quad (\text{A1})$$

and

$$\int d\Omega \mathbf{X}_{l'm'}^*(\Omega) \cdot \nabla \times [(a_j j_l(kr) + b h_l(kr)) \mathbf{X}_{lm}(\Omega)] = 0, \quad (\text{A2})$$

for the vector spherical harmonics, that

$$ka_{lm}^{(M)} j_l(kr) = \int d\Omega (\mathbf{X}_{lm})^* \cdot \mathbf{E}. \quad (\text{A3})$$

To calculate $a_{lm}^{(E)}$, it is easier to use the overlap between the \mathbf{B} field and a vector spherical harmonic,

$$\frac{k}{c} a_{lm}^{(E)} j_l(kr) = \int d\Omega (\mathbf{X}_{lm})^* \cdot \mathbf{B}. \quad (\text{A4})$$

To evaluate these surface integrals, we use the expansion of a scalar plane wave (i.e. the factor $e^{i\mathbf{q}\cdot\mathbf{r}}$) in terms of spherical harmonics and insert this in Eq. (2.1) yielding

$$\begin{aligned} \mathbf{E}(\mathbf{r}) &= \left\{ E^{(s)} [\hat{\mathbf{z}} \times \hat{\mathbf{q}}_{\parallel}] - E^{(p)} [\hat{\mathbf{q}} \times (\hat{\mathbf{z}} \times \hat{\mathbf{q}}_{\parallel})] \right\} e^{i\mathbf{q}\cdot\mathbf{R}_{\text{sph}}} \\ &\times 4\pi \sum_{l=0}^{\infty} i^l j_l(kR) \sum_m (-1)^m Y_{l,-m}(\Omega) Y_{l,m}(\Omega_q). \end{aligned} \quad (\text{A5})$$

The incident B field can be expanded in a similar way. The factor $e^{i\mathbf{q}\cdot\mathbf{R}_{\text{sph}}}$ compensates for the fact that we here use a coordinate system with the origin at the center of

the sphere [$\mathbf{R}_{\text{sph}} = -\hat{\mathbf{z}}(R+d)$]. The composite variables Ω and Ω_q denote the directions of $\hat{\mathbf{r}}$ (i.e. the angles θ and ϕ) and $\hat{\mathbf{q}}$ (θ_q and ϕ_q). Equation (A5) is also valid for evanescent waves that decay exponentially in the positive or negative z direction in which case $\cos\theta_q$ is purely imaginary. From the definition in Eq. (2.20) and the fact that \mathbf{L} can be written in terms of ladder operators as

$$\mathbf{L} = \frac{1}{2}(\hat{\mathbf{x}} - i\hat{\mathbf{y}})L_+ + \frac{1}{2}(\hat{\mathbf{x}} + i\hat{\mathbf{y}})L_- + \hat{\mathbf{z}}L_z,$$

it is clear that \mathbf{X}_{lm} can be expressed in terms of the spherical harmonics $Y_{l,m+1}$, $Y_{l,m}$, and $Y_{l,m-1}$. Combining this with the expansion in Eq. (A5) yields the overlap integrals

$$f_{lm}^{Ep}(\mathbf{q}) = f_{lm}^{Ms}(\mathbf{q}) = k^{-1} U_{lm}(\mathbf{q}) e^{i\mathbf{q}\cdot\mathbf{R}_{\text{sph}}}, \quad (\text{A6})$$

and

$$f_{lm}^{Es}(\mathbf{q}) = -f_{lm}^{Mp}(\mathbf{q}) = k^{-1} V_{lm}(\mathbf{q}) e^{i\mathbf{q}\cdot\mathbf{R}_{\text{sph}}}. \quad (\text{A7})$$

Here we have introduced

$$\begin{aligned} U_{lm}(\mathbf{q}) &= -\frac{2\pi i^l (-1)^m}{\sqrt{l(l+1)}} [\xi_+ F_+(l, m) Y_{l,-m-1}(\Omega_q) + \\ &+ \xi_- F_-(l, m) Y_{l,-m+1}(\Omega_q)], \end{aligned} \quad (\text{A8})$$

where the polarization vector

$$\begin{aligned} \hat{\xi} &= \hat{\mathbf{z}} \times \hat{\mathbf{q}}_{\parallel} = \hat{\mathbf{y}} \cos\phi_q - \hat{\mathbf{x}} \sin\phi_q, \quad \text{with} \\ \xi_{\pm} &\equiv \xi_x \pm i\xi_y = \pm i e^{\pm i\phi_q}. \end{aligned} \quad (\text{A9})$$

In a similar way

$$\begin{aligned} V_{lm}(\mathbf{q}) &= -\frac{2\pi i^l (-1)^m}{\sqrt{l(l+1)}} [\eta_+ F_+(l, m) Y_{l,-m-1}(\Omega_q) + \\ &+ \eta_- F_-(l, m) Y_{l,-m+1}(\Omega_q) - \eta_z 2m Y_{l,-m}(\Omega_q)], \end{aligned} \quad (\text{A10})$$

where the polarization vector

$$\begin{aligned} \hat{\eta} &= k^{-1} \mathbf{q} \times (\hat{\mathbf{z}} \times \hat{\mathbf{q}}_{\parallel}) \\ &= \hat{\mathbf{x}}(-\cos\theta_q \cos\phi_q) + \hat{\mathbf{y}}(-\cos\theta_q \sin\phi_q) + \hat{\mathbf{z}} \sin\theta_q, \quad \text{with} \\ \eta_{\pm} &\equiv \eta_x \pm i\eta_y = -\cos\theta_q e^{\pm i\phi_q}. \end{aligned} \quad (\text{A11})$$

In both Eq. (A8) and Eq. (A10), F_+ and F_- are shorthand symbols for the numerical factors produced by the ladder operators L_+ and L_- , thus

$$\begin{aligned} F_+(l, m) &= \sqrt{(l-m)(l+m+1)}, \quad \text{and} \\ F_-(l, m) &= \sqrt{(l+m)(l-m+1)}. \end{aligned} \quad (\text{A12})$$

Finally, we note that the ϕ_q dependence of both U_{lm} and V_{lm} follows

$$U_{lm}(\mathbf{q}) \propto e^{-im\phi_q}, \quad V_{lm}(\mathbf{q}) \propto e^{-im\phi_q}. \quad (\text{A13})$$

The same is true for f_{lm} (provided \mathbf{R}_{sph} lies on the z axis).

Next we must deal with the overlap going in the other direction, from a given multipole to a plane wave. The vector equivalents of the Kirchoff integrals provides one way of doing this. They read

$$\mathbf{E}(\mathbf{r}) = \mathbf{E}^{\text{ext}}(\mathbf{r}) + \int dS' [ikc(\hat{\mathbf{n}}' \times \mathbf{B}(\mathbf{r}'))G(\mathbf{r}, \mathbf{r}') + (\hat{\mathbf{n}}' \times \mathbf{E}(\mathbf{r}')) \times \nabla'G + (\hat{\mathbf{n}}' \cdot \mathbf{E}(\mathbf{r}'))\nabla'G] \quad (\text{A14})$$

and

$$\mathbf{B}(\mathbf{r}) = \mathbf{B}^{\text{ext}}(\mathbf{r}) + \int dS' \left[-\frac{ik}{c}(\hat{\mathbf{n}}' \times \mathbf{E}(\mathbf{r}'))G(\mathbf{r}, \mathbf{r}') + (\hat{\mathbf{n}}' \times \mathbf{B}(\mathbf{r}')) \times \nabla'G + (\hat{\mathbf{n}}' \cdot \mathbf{B}(\mathbf{r}'))\nabla'G \right]. \quad (\text{A15})$$

Here G denotes the Green's function of the scalar Helmholtz equation in free space, thus G solves

$$[\nabla^2 + k^2]G(\mathbf{r}, \mathbf{r}') = -\delta^{(3)}(\mathbf{r} - \mathbf{r}'), \quad (\text{A16})$$

where $k = \omega/c$, and can be written

$$G(\mathbf{r}, \mathbf{r}') = \frac{e^{ik|\mathbf{r}-\mathbf{r}'|}}{4\pi|\mathbf{r}-\mathbf{r}'|}. \quad (\text{A17})$$

To get the total field at a point in free space, the integrals in Eqs. (A14) and (A15) should be over the surfaces of all the scatterers that are present, and the fields entering the integrals should be the exact fields at those interfaces. Here we restrict the attention to the fields scattered from the sphere. In that case, only the Hankel function terms in Eqs. (2.18) and (2.19) contribute. Evaluating the surface integrals using an expansion of the Green's function in terms of plane waves (propagating and evanescent),

$$G(\mathbf{r}, \mathbf{r}') = i \int \frac{d^2q_{\parallel}}{(2\pi)^2} \frac{e^{i\sqrt{k^2 - q_{\parallel}^2}|z-z'|}}{2\sqrt{k^2 - q_{\parallel}^2}} e^{i\mathbf{q}_{\parallel} \cdot (\mathbf{r}_{\parallel} - \mathbf{r}'_{\parallel})}, \quad (\text{A18})$$

one finds that the field outside the sphere can be written

$$\mathbf{E} = \sum_{lm, \sigma} b_{lm}^{\sigma} \int \frac{d^2q_{\parallel}}{(2\pi)^2} \times [g_{lm}^{s\sigma}(\mathbf{q})(\hat{\mathbf{z}} \times \hat{\mathbf{q}}_{\parallel}) - g_{lm}^{p\sigma}(\mathbf{q})(\hat{\mathbf{q}} \times (\hat{\mathbf{z}} \times \hat{\mathbf{q}}_{\parallel}))] e^{i\mathbf{q} \cdot \mathbf{r}}. \quad (\text{A19})$$

Here σ denotes a polarization [(E) or (M)]. The coupling factors are found to be

$$g_{lm}^{pE}(\mathbf{q}) = g_{lm}^{sM}(\mathbf{q}) = \frac{(-1)^{l+m+1} e^{-i\mathbf{q} \cdot \mathbf{R}_{\text{sph}}}}{2\sqrt{k^2 - |\mathbf{q}_{\parallel}|^2}} U_{l, -m}(\mathbf{q}), \quad (\text{A20})$$

and

$$g_{lm}^{sE}(\mathbf{q}) = -g_{lm}^{pM}(\mathbf{q}) = \frac{(-1)^{l+m+1} e^{-i\mathbf{q} \cdot \mathbf{R}_{\text{sph}}}}{2\sqrt{k^2 - |\mathbf{q}_{\parallel}|^2}} V_{l, -m}(\mathbf{q}), \quad (\text{A21})$$

where \mathbf{R}_{sph} is a vector pointing to the center of the sphere. As for the ϕ_q dependence of g_{lm} , it is in view of Eq. (A13) clear that

$$g_{lm}^{\sigma\sigma'} \propto e^{im\phi_q}.$$

* Electronic address: peter.johansson@teorfys.lu.se

† Electronic address: apell@fy.chalmers.se

‡ Electronic address: david.penn@nist.gov

¹ Within the theory we will present here, the resolution would mainly be determined by the size of the electromagnetic cavity formed between the tip and sample. This leads to a resolution limit of the order of 5–10 nm. The 1nm resolution has been obtained in STM light emission experiments by R. Berndt (private communication) that make use of very sharp tips.

² A. L. Vázquez de Parga and S. F. Alvarado, Phys. Rev. Lett. **72**, 3726 (1994).

³ N. Majlis, A. Levy Yeyati, F. Flores, and R. Monreal, Phys. Rev. B **52**, 12505 (1995).

⁴ D. T. Pierce, A. Davies, J. A. Stroschio, and R. J. Celotta, Appl. Phys. A **66**, S403 (1998).

⁵ S. P. Apell, D. R. Penn, and P. Johansson, Phys. Rev. B **61**, 3534 (2000).

⁶ T. J. Silva and S. Schultz, Rev. Sci. Instrum. **67**, 715 (1996).

⁷ I. I. Smolyaninov, A. V. Zayats, and C. C. Davis, Optics Letters **22**, 1592 (1997).

⁸ L. Aigouy, S. Gresillon, A. C. Boccara, J. C. Rivoal, V. Mathet, C. Chappert, J. P. Jamet, and J. Ferre, Journal of Microscopy-Oxford **194**, 295 (1999).

⁹ R. Wiesendanger, H.-J. Güntherodt, G. Güntherodt, R. J. Gambino, and R. Ruf, Phys. Rev. Lett. **65**, 247 (1990).

¹⁰ S. Heinze, M. Bode, A. Kubetzka, O. Pietzsch, X. Nie, S. Blügel, and R. Wiesendanger, Science **288**, 1805 (2000).

¹¹ J. D. Jackson, *Classical Electrodynamics* (Wiley, New York, 1999).

¹² We use a local dielectric function. Nonlocal effects are small and would not change the results of this calculation in any considerable way. For a more detailed discussion of this, see Sec. IV D of Ref. 15.

¹³ J. Zak, E. R. Moog, C. Liu, and S. D. Bader, Phys. Rev. B **43**, 6423 (1991); **46**, 5883 (E) (1992).

¹⁴ M. B. Stearns, in *Magnetic Properties of Metals*, Landolt-Börnstein New Series Group III, Vol. 19, Pt. a, edited by H. P. J. Wijn (Springer-Verlag, Berlin, 1986), pp. 113.

¹⁵ P. Johansson, Phys. Rev. B **58**, 10 823 (1998).

¹⁶ Note that strictly speaking there are contributions in Eqs. (2.38) and (2.39) that are second order in ϵ_1 . They are, however, negligibly small.

¹⁷ The quantity $D(\omega)$ was denoted $K(\omega)$ in Ref. 5.

¹⁸ T. Junno, K. Deppert, L. Montelius, and L. Samuelson, Appl. Phys. Lett. **66**, 3627 (1995).

¹⁹ M. R. Pufall, A. Berger, and S. Schultz, J. Appl. Phys. **81**, 5689 (1997).

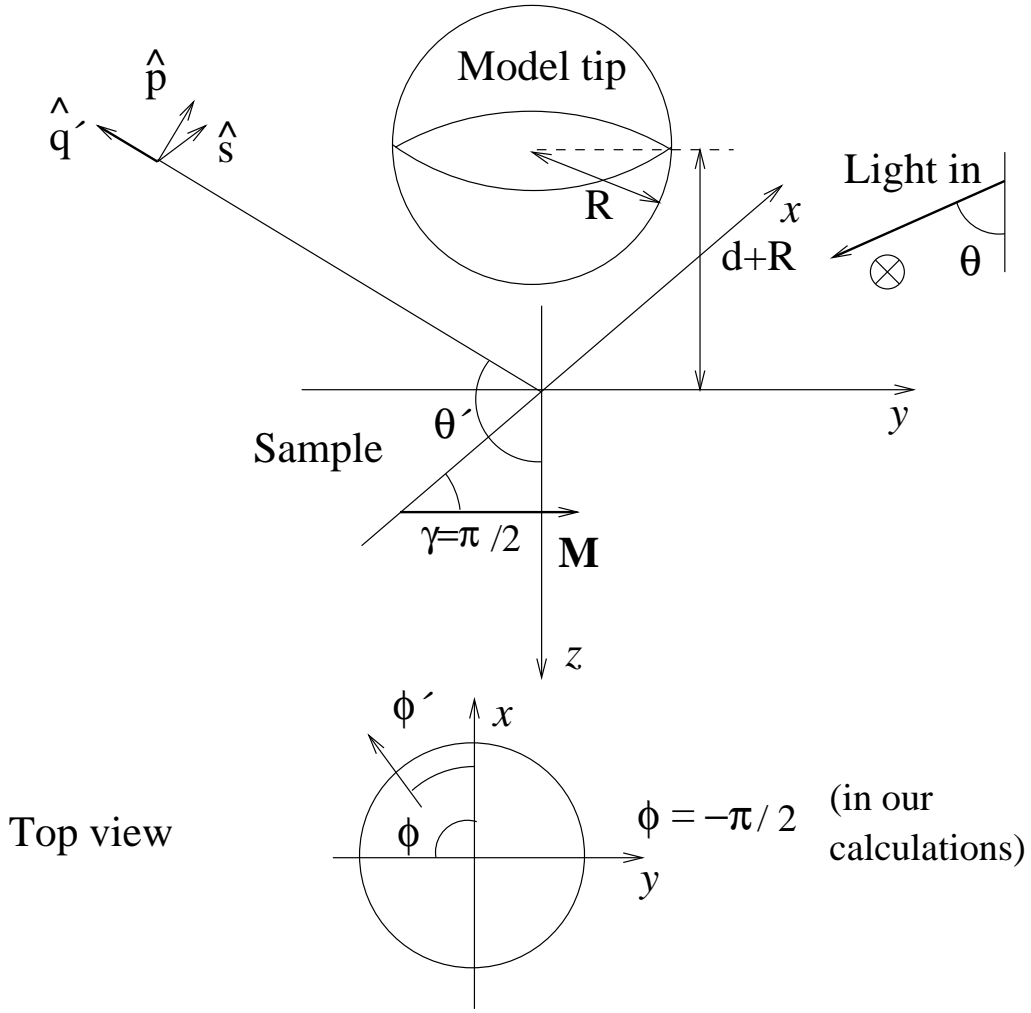


FIG. 1. The model geometry used in the calculation. The vectors $\hat{\mathbf{q}}'$, $\hat{\mathbf{p}}$, and $\hat{\mathbf{s}}$ indicate propagation and polarization directions in the radiation zone. θ and ϕ and θ' and ϕ' are the angles of incidence and observation, respectively, in a spherical coordinate system.

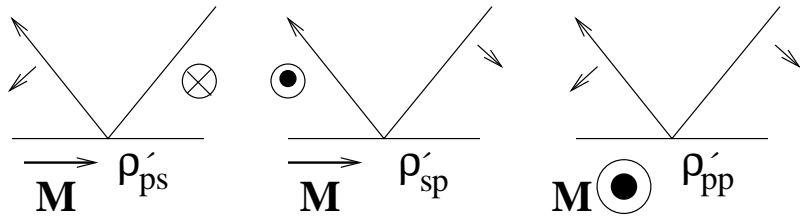


FIG. 2. Illustration of the different “anomalous” scattering processes involving the Kerr effect that can take place at the sample surface. Conversion of s to p polarization and vice versa is most effective when the in-plane component of the wave vector is collinear with the sample magnetization \mathbf{M} . However, the Kerr contribution to the p to p reflection is most effective when \mathbf{q}_{\parallel} and \mathbf{M} are perpendicular (NB. In the figure to the right the viewpoint, but not the magnetization differs from the other figures).

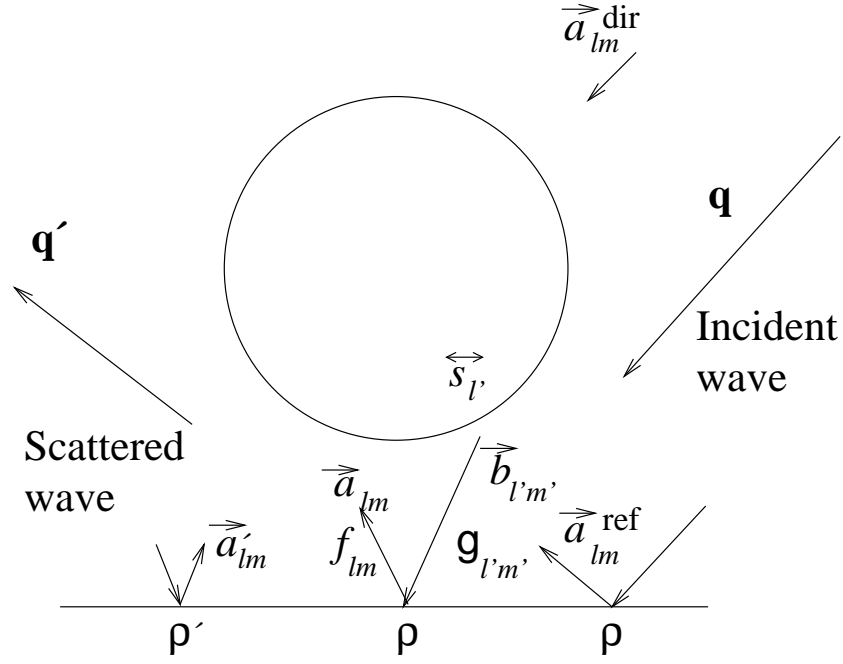
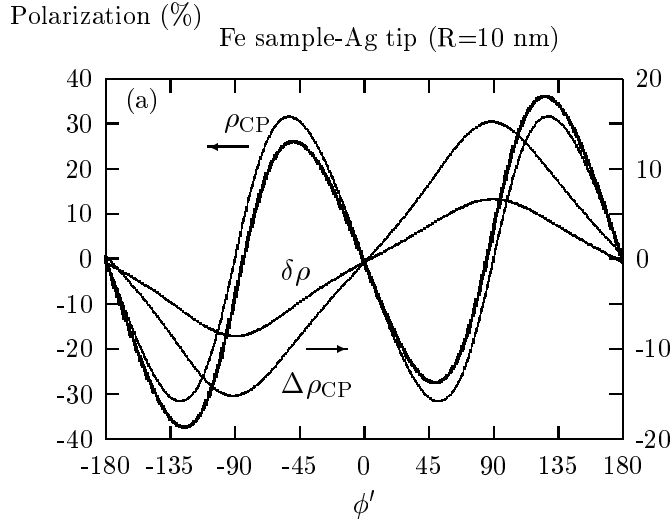
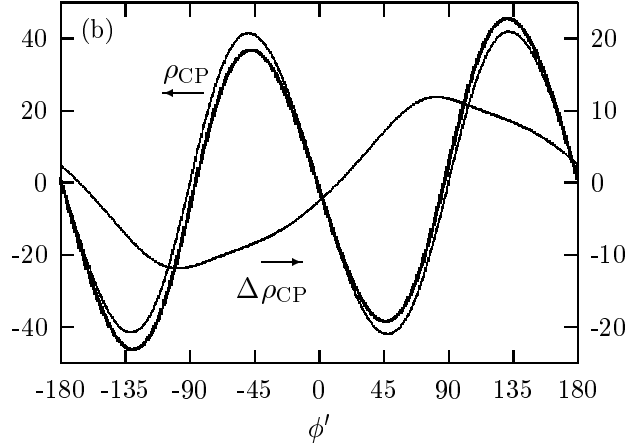


FIG. 3. Illustration of the general scheme employed in the calculation. An incident plane wave can be expressed as a multipole expansion of waves impinging on the sphere, either directly ($\vec{a}_{lm}^{\text{dir}}$) or after an initial reflection off the sample ($\vec{a}_{lm}^{\text{ref}}$). Subsequently, multiple scattering takes place between the sphere and the sample. The sphere response functions s determines the strength of the outgoing spherical waves $\vec{b}_{l'm'}$, which can be expanded into plane waves according to the functions $g_{l'm'}$ and after reflection off the sample (governed by ρ), the functions f_{lm} determine the strengths \vec{a}_{lm} of the different multipole contributions to the reflected wave that again impinges on the sphere. Anomalous (Kerr effect) reflections which are governed by the functions ρ' generate waves incident on the sphere with strength \vec{a}'_{lm} .



Polarization (%) Fe sample-Ag tip (R=20 nm)



Polarization (%) Fe sample-W tip (R=10 nm)

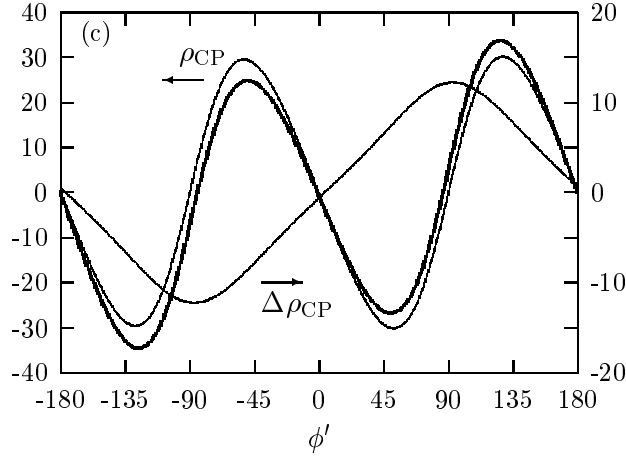


FIG. 4. Calculated degree of polarization for a Ag tip probing a Fe sample. The curves in panel (a) were calculated with a tip radius $R = 10$ nm, the ones in panel (b) with $R = 20$ nm. For comparison results calculated with a W tip with $R = 10$ nm are displayed in panel (c). In all cases the tip-sample separation $d = 0.5$ nm. The photon energy was set to 1.6 eV, $\phi = -90^\circ$, and the polar angles of incidence and observation θ and θ' , respectively, both lie 1 radian off the surface normal (i.e. $\theta = 1$ rad. while $\pi - \theta' = 1$ rad.). The two curves with the highest amplitude show the results for ρ_{CP} . The thinner of these curves was calculated without accounting for the magneto-optic properties of the sample, whereas they have been included in the calculation yielding the thicker curve. The remaining curves display (i) the quantity $\Delta\rho_{CP}$ defined in Eq. (3.13), and (ii), in panel (a), the difference $\delta\rho$ between the results with and without magneto-optic effects.

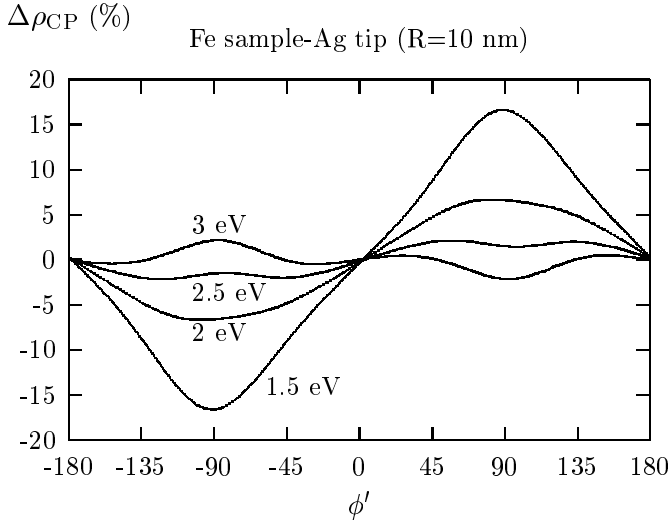


FIG. 5. The polarization asymmetry $\Delta\rho_{CP}$, defined in Eq. (3.13), plotted as a function of observation angle ϕ' , for a number of photon energies for a Fe sample scanned by a Ag tip with a radius of 10 nm, and with d set to 0.5 nm.

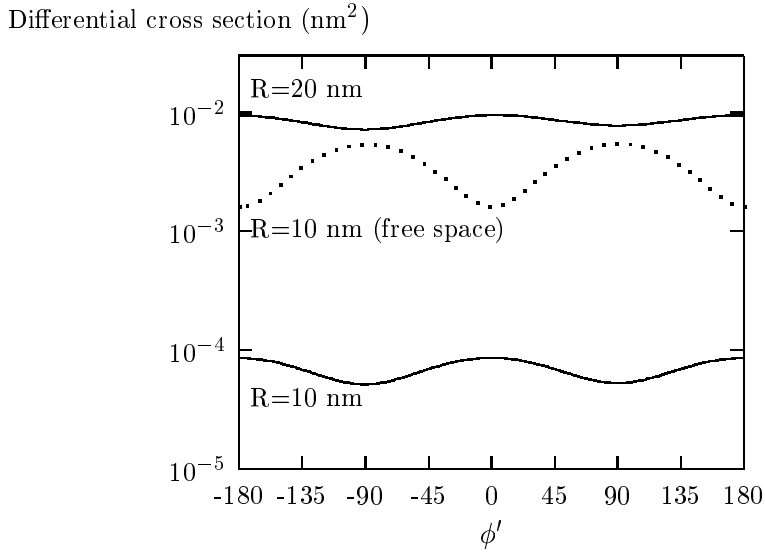


FIG. 6. Calculated differential scattering cross section for a Ag sphere in front of a Fe sample (full curves), and in free space (dotted curve) as a function of azimuthal observation angle. The photon energy is 1.6 eV, $d = 0.5$ nm, the sphere radius is 10 nm (lower full curve and dotted curve), and 20 nm (upper full curve), respectively. The polar angles of incidence and observation θ and θ' , respectively, both lie 1 radian off the surface normal (i.e. $\theta = 1$ rad. while $\pi - \theta' = 1$ rad.).

TABLE I. The off-diagonal element $\epsilon_1(\omega)$ of the dielectric tensor for Fe and Co for a few photon energies. The data are taken from Ref. 14.

$\hbar\omega$ (eV)	Fe	Co
1.5	-1.42-0.089i	-1.16-0.089i
2.0	-0.67-0.26i	-0.40-0.15i
2.5	-0.26-0.22i	-0.20-0.096i
3.0	-0.13-0.12i	-0.10-0.067i